Pergamon

Chaos, Solitons & Fractals Vol. 5, No. 10, pp. 2047–2053, 1995
Elsevier Science Ltd
Printed in Great Britain.

0960–0779(94)00181-2

Large-scale Structure in Rayleigh–Bénard Convection with Impenetrable Sidewalls

ROBERT M. KERR, JACKSON R. HERRING and AXEL BRANDENBURG

Geophysical Turbulence Program, National Center for Atmospheric Research, P.O. Box 3000, Boulder, CO 80307, USA

Abstract—In numerical Rayleigh–Bénard convection at Rayleigh number 10^5 and 5×10^5, Prandtl numbers 0.07, 0.7, and 7, and aspect ratios 3, 4 or 6, large-scale patterns are sought. For aspect ratio 6 and $Pr = 0.7$, saturation of the mean velocity is only observed after 20 convective timescales. Three-dimensional visualization shows a strong influence of the confining sidewalls and corners for all Prandtl numbers. Sweeping motions are observed for $Pr = 7$.

1. INTRODUCTION

A common feature of most experimental Rayleigh–Bénard experiments is the appearance of large-scale flows, for aspect ratios, that is width/height, as large as 10 [1, 2]. Here, a large-scale flow means organized flow over the entire domain, that is the horizontal scale is much larger than the typical size of convection cells. While a large-scale flow might be the asymptotic state, it can take up to 100 convective timescales to appear [1]. Careful work has been done with aspect ratio 10 to demonstrate that the effect is not related to spurious effects such as a slight tilt in the experimental device [1]. The large-scale flow is not observed in a recent experiment with aspect ratio 30 (Busse, private communication). While there is *a priori* no reason to expect large-scale flows from linear analysis [3], some recent theoretical studies [4]–[6] of convection suggest the possibility. First, in a highly truncated nonlinear model [4] the modes for a large-scale shear can be finite. More recently [6] a large-scale flow is used to explain the appearance of anomalous scaling exponents in the high Rayleigh number hard-turbulence regime.

Numerical work on time-dependent convection with rigid upper and lower plates has found large-scale patterns at low aspect ratio. In a small aspect ratio two-dimensional box with impenetrable, free-slip sidewalls [7] it has been demonstrated that large-scale flows similar in appearance to experimental three-dimensional flows form. Three-dimensional simulations in this geometry by DeLuca and Cattaneo (unpublished) also support the appearance of large-scale flows. However, in a large-aspect-ratio three-dimensional simulation with rigid upper and lower plates and periodic sidewalls [8], significant mean horizontal velocities are observed, yet no evidence of a large-scale structure is found. This calculation [8] suggests that the mean velocity in small-aspect-ratio calculations is a artifact of the small sample size due to the small number of convective cells in the computational domain. Moreover, it does not seem necessary to have a large-scale flow to get the anomalous scaling dependence of normalized heat flux, or Nusselt number, on Rayleigh number of $Nu \approx Ra^{2/7}$ seen experimentally [9]. Instead it is sufficient to have a large local shear due to large convective cells. The question then arises of what particular physics separates the large-aspect-ratio, periodic simulations [8] from the small-aspect-ratio,

two-dimensional simulations [7] and the experiments [9]. The purpose of this paper is to begin to investigate possible sources for these differences.

2. SIMULATIONS

What will be investigated in this report is the effect of impenetrable, free-slip side walls and varying Prandtl number. Continuing work is investigating varying Rayleigh number and aspect ratio. Free-slip sidewalls are chosen because the existing two- and three-dimensional small aspect ratio simulations with free-slip sidewalls have already demonstrated that a single cell will develop for those simulations. In unpublished studies with periodic sidewalls and small aspect-ratio, we have found no evidence for a large-scale flow for aspect ratio greater than 2 and for aspect-ratio less than 1.5 the large-scale shear appeared only intermittently. The simulations reported here will have aspect ratio 3, 4 or 6.

The nondimensional equations to be represented are the incompressible Navier–Stokes equations in the Boussinesq approximation between two walls.

$$\frac{\partial \mathbf{u}}{\partial t} + \mathbf{u}\cdot\nabla\mathbf{u} = -\nabla P + Ra\theta + Pr\,\nabla^2\mathbf{u}$$

$$\frac{\partial \theta}{\partial t} + \mathbf{u}\cdot\nabla\theta = \nabla^2\theta$$

$$\nabla\cdot\mathbf{u} = 0$$

where $\mathbf{u} = (u, v, w)$, θ is the temperature, and the dimensionless coefficients Ra and Pr are the Rayleigh number expressing the strength of thermal forcing and the Prandtl number, the ratio of kinematic viscosity and thermal diffusivity, ν/κ. x and y are the horizontal directions varying between 0 and L and z is the vertical, varying between -1 and 1, yielding an aspect ratio AR of $L/2$. In the vertical, the velocity boundary conditions are rigid

$$u = v = w = \frac{\partial w}{\partial z} = 0$$

and the temperature is fixed

$$\theta|_{z=\pm 1} = \mp 1.$$

In the horizontal, the velocity boundary conditions are no-stress and the temperature boundary conditions are no-flux. At $x = 0, L$ this is

$$u = \frac{\partial v}{\partial x} = \frac{\partial w}{\partial x} = \frac{\partial \theta}{\partial x} = 0$$

and at $y = 0, L$ this is

$$v = \frac{\partial u}{\partial y} = \frac{\partial w}{\partial y} = \frac{\partial \theta}{\partial y} = 0.$$

The numerical method uses sine and cosine transforms in the horizontal xy to represent the free-slip, no-flux boundary conditions in the horizontal. In the vertical z, Tchebyshev polynomials are used to represent the no-slip, constant temperature boundaries. Incompressibility and the boundary conditions are satisfied on each timestep using a poloidal–toroidal decomposition of the velocity and expansion functions that match the boundary conditions. The operating parameters are relevant dimensionless numbers for the simulations are given in Table 1. In this preliminary investigation low Rayleigh numbers using

Table 1. Summary of the numerical simulations

Mesh	AR	Ra	Pr	R_λ	Nu
64 × 64 × 32	6	10^5	0.7	15	4.5
32 × 32 × 32	3	10^5	0.07	60	3.5
32 × 32 × 32	3	10^5	0.7	15	4.5
32 × 32 × 32	3	10^5	7.0	2	5.5
64 × 64 × 64	4	5×10^5	0.07	50	5.5
64 × 64 × 64	4	5×10^5	0.7	25	6.8
64 × 64 × 64	4	5×10^5	7.0	4	7.2

small meshes are being studied in order to simulate a large number of convective timescales. $Pr = 7$ represents water, $Pr = 0.7$ represents a gas, and $Pr = 0.07$ was chosen as the smallest Prandtl number that could be easily simulated.

For fixed Rayleigh number, the Taylor microscale Reynolds number R_λ depends strongly on Prandtl number. Since a Taylor microscale Reynolds number of about 15 is generally regarded as marginally turbulent, for $Pr = 0.7$ a Reynolds number of $Ra = 10^5$ would be consistent with the Rayleigh number of the appearance of 'hard' turbulence 2/7 scaling in large-aspect-ratio experiments [2] and the first indications of turbulent enstrophy production [8]. Note that this is a much lower Rayleigh number than in the original low-aspect-ratio experiments [9].

For fixed Rayleigh number, Nusselt number also has some Prandtl number dependence. The trend is for Nusselt number to increase with Prandtl number, contrary to the prediction of [6], but in agreement with earlier calculations with free-slip upper and lower boundaries [10]. But the Reynolds numbers of these simulations are far too low to provide any true comparison with their theory.

3. STRUCTURES

A typical profile of the horizontally averaged x-velocity $\langle u \rangle$ is shown in Fig. 1. Note the distinct extrema at $z = \pm 0.5$. Using *top* and *bot* to indicate top and bottom, we define the corresponding average velocities at these maximal points to be $\langle u_{top} \rangle$ and $\langle u_{bot} \rangle$, 0.0195 and -0.015 in this case respectively, and similarly for $\langle v \rangle$. Then to help determine whether there is a large-scale flow we use the following measure of mean velocity

$$\frac{|\langle u_{top} \rangle| + |\langle u_{bot} \rangle| + |\langle v_{top} \rangle| + |\langle v_{bot} \rangle|}{u_{rms}}$$

To compare dimensionless time, we define a convective timescale as $8/u_{rms}$, where a length of 8 is the circuit around a unit aspect ratio convection cell with a height of 2.

For the simulation with $Ra = 10^5$, $Pr = 0.7$ and aspect ratio 6 this measure of relative mean velocity increases from a value of 0.1 after one convective timescale to 0.4 after 20 convective timescales, with saturation indicated after that until the final time of 40 convective timescales. For comparison, $u_{\rm rms}$, which is related kinetic energy, saturates after less than 1/2 a convective timescale, so the increase in relative mean velocity is entirely due to an increase in the mean velocity. For this simulation, this measure of the mean velocity is roughly 3 to 4 times the value obtained in simulation with periodic boundary run after 20 convective timescales. Therefore, the confining boundaries are increasing the mean flow. But does this indicate a large-scale pattern?

Figure 2 is a three-dimensional visualization of the simulation for $Pr = 7$, $Ra = 10^5$, aspect ratio 3 after 8.4 convective timescales. Note the strong horizontal vorticity on the

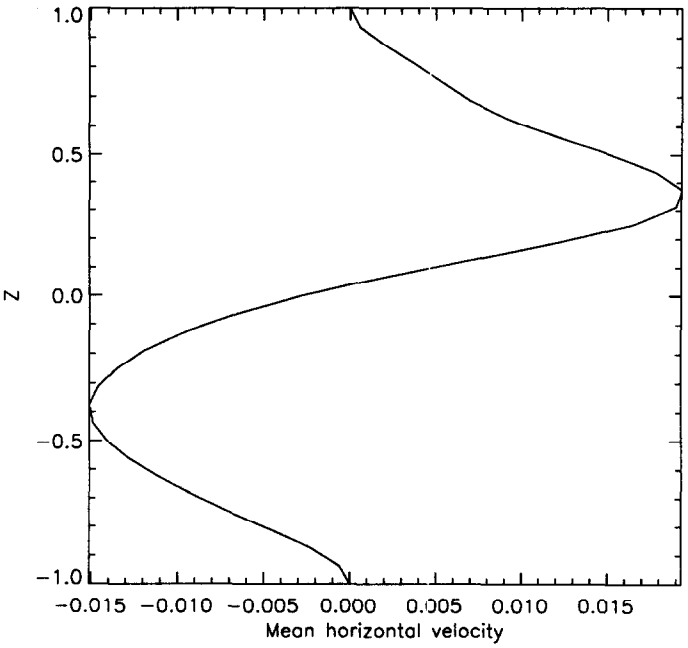

Fig. 1. Two typical profiles of $\langle a \rangle$, average x-horizontal velocity for $AR = 6$, $Ra = 10^8$, $Pr = 0.1$ calculation.

lower wall in rings around where major downdrafts splat into the lower surface. Comparatively, there is little vertical vorticity associated with the major up and down drafts.

Figure 2 was chosen because it demonstrates all the major features seen in visualizations of the lower Prandtl number simulations for $Ra = 10^5$. First, a strong alignment with the corners and diagonals should be apparent, but there is no large-scale flow. The influence of the confining boundaries can appear in two dimensional surface plots as large up or down drafts across an entire horizontal wall, which can give an impression of a large-scale flow. But there are still multiple cells, which is not what is reported for the experimental observations. Some alignment with the diagonals persists for several convective timescales in all the calculations, but eventually breaks down. Still, a persistent influence from the sidewalls is always apparent. How these flow structures can be related to the increase in mean velocity is unclear.

A possibly significant difference between the visualization of $Pr = 7$ calculation and the lower Prandtl number calculations is the appearance of sweeping along the lower right vertical sidewall. That is, the motion of warm fluid along the lower boundary, indicated by the red arrows, is largely horizontal. This is the type of flow seen experimentally, but the persistence of the major plumes in the interior of Fig. 2 implies that this simulation is still not showing a large-scale flow. For $Pr = 0.7$ sweeping motion of this type is never seen, the flow is totally dominated by plumes with strong alignment with the boundaries and corners. For $Pr = 0.07$ the flow is similar to $Pr = 0.7$, except the plumes are broader due to the increased thermal diffusivity.

The sweeping motion in Fig. 2 is the one indication of dynamics possibly consistent with large-scale flow in these calculations. Sweeping is found for both Rayleigh number calculations $Ra = 10^5$, 5×10^5 at $Pr = 7$. It is still possible that if these simulations are run for 10 or more convective timescales, the length of time that it seems was required to reach saturation for the $Ra = 10^5$, $Pr = 0.7$, aspect ratio 6 calculation, that a true large-scale flow

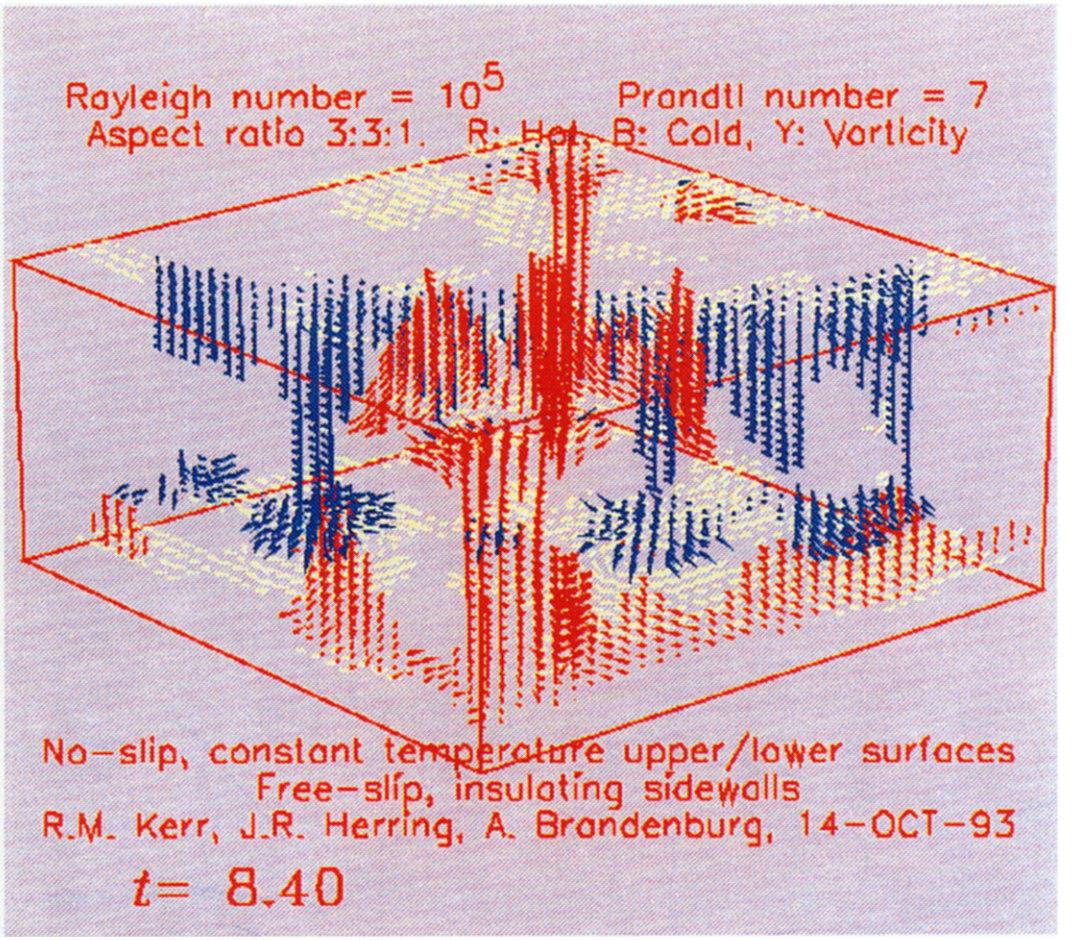

Fig. 2. Three-dimensional visualization of the simulation for $Pr = 7$, $Ra = 10^5$, aspect ratio 3 after 8.4 convective timescales. Red and blue arrows represent up and down drafts respectively. The arrows are chosen based on the fluctuation temperature so that the solid hot or cold regions near the boundaries would not obscure the interior. The direction and length of the arrows is based on the velocity at the points. Yellow is used to indicate large vorticity, with the arrows chosen based on vorticity squared and the length and direction of the arrows based on the local vorticity.

might develop. These calculations are currently in progress, but it would be useful to consider why some sweeping motion has already been observed.

4. CONCLUSION

In this paper, the Prandtl number dependence of Rayleigh–Bénard convection with impenetrable sidewalls has been investigated. Significant sweeping motions occur for large Prandtl numbers and qualitatively resemble large-scale features observed in laboratory experiments. One explanation for the sweeping in the $Pr = 7$ calculation might be that since the viscosity is larger than the thermal diffusivity, the momentum boundary layer is thicker. This argument might also apply to the experimental observations. It should be noted that there have never been any experimental visualizations of large-scale flow in large-aspect-ratio experiments using a gas, that is $Pr = 0.7$. All the visualizations have been in water tank experiments. It is possible that high Prandtl number is required to obtain a flow encompassing the entire tank at large aspect ratio. This does not imply that a gas with $Pr = 0.7$ could not have large rolls and significant local shear that might be sufficient to produce hard turbulent scaling without a large-scale flow.

Acknowledgement—The National Center for Atmospheric Research is sponsored by the National Science Foundation.

REFERENCES

1. R. Krishnamurti and L. N. Howard, Large-scale flow generation in turbulent convection. *Proc. Nat. Acad. Sci.* **78**, 1981–1985 (1981).
2. X. Z. Wu and A. Libchaber, Scaling relations in thermal turbulence: The aspect-ratio dependence, *Phys. Rev. A* **45**, 842–845 (1992).
3. S. Chandrasekar, *Hydrodynamic and Hydromagnetic Stability*. Clarendon Press, Oxford (1961).
4. L. N. Howard and R. Krishnamurti, Large-scale flow in turbulent convection: a mathematical model. *J. Fluid Mech.* **170**, 385–410 (1986).
5. J. M. Massaguer, E. A. Spiegel and J. P. Zahn, Convection-induced shears for general planforms, *Phys. Fluids A* **4**, 1333–1335 (1992).
6. B. I. Shraiman and E. Siggia, Heat transport in high Rayleigh number convection, *Phys. Rev. A* **42**, 3650–3653 (1991).
7. J. Werne, E. E. DeLuca, R. Rosner and F. Cattaneo, Development of hard-turbulent convection in two dimensions: Numerical evidence, *Phys. Rev. Lett.* **67**, 3519–3522 (1990).
8. R. M. Kerr, Simulation of high Rayleigh number convection, Submitted to *J. Fluid. Mech.* (1992).
9. F. Heslot, B. Castaing and A. Libchaber, Transition to turbulence in helium gas, *Phys. Rev. A* **36**, 5870–5873 (1987).
10. J. R. Herring and S. Jackson, Thermal convection: Numerical experiments near the onset to turbulence and the statistical theory of turbulence, in *Turbulence and Chaotic Phenomena in Fluids* edited by T. Tatsumi, IUTAM 111–116. North-Holland, Amsterdam (1984).